Hindawi
Geofluids
Volume 2022, Article ID 1880502, 12 pages
https://doi.org/10.1155/2022/1880502

Research Article

DEM Analysis and Simplified Calculation of Passive Earth Pressure on Retaining Walls Backfilled with Sand Considering Strain-Softening Behavior

Minghui Yang,[1,2] **Hutao Gong**,[1] **and Bo Deng**[3]

[1]*College of Civil Engineering, Hunan University, Changsha, Hunan 410082, China*
[2]*Department of Civil Engineering, Xiamen University, Xiamen, Fujian Province 361005, China*
[3]*College of Civil Engineering, University of South China, Hengyang, Hunan Province 421001, China*

Correspondence should be addressed to Bo Deng; parl_d@126.com

Received 22 April 2022; Accepted 9 May 2022; Published 9 June 2022

Academic Editor: Di Feng

Common calculation methods of passive earth pressure, such as the Rankine or Coulomb earth pressure theory, assume that the width of the fill behind the wall is sufficient for the development of the slip surface and that after the passive earth pressure reaches the limit state, its value remains unchanged with the increase of displacement of the retaining wall. Nevertheless, cases with narrow backfill width should be considered when retaining walls must be built close to existing stabilization walls in urban areas or near rock faces in mountainous areas. Furthermore, for sand, especially dense sand, when the displacement of the retaining wall is large, a strain-softening behavior similar to the triaxial test will appear, resulting in a decrease in passive earth pressure. In this regard, a practical model for strain-softening of dense sand is proposed firstly and verified by the discrete element method (DEM) using the Particle Flow Code (PFC-2D) software. Then, based on the sliding surface shape obtained by DEM, a simplified method for determining the passive earth pressure distribution of retaining walls using limit equilibrium analysis was proposed. Finally, the passive earth pressures calculated by the proposed method agree well with those from PFC results, and the effects of the width of the backfill and displacement of retaining wall on the distribution of active earth pressure were discussed.

1. Introduction

With the increasing density of urban buildings and the increasing shortage of construction land, the distance between many excavated foundation pits and the walls of existing underground buildings is very close, resulting in narrow backfill between them. In the design of foundation pit engineering, the calculation of earth pressure is very key, which directly determines the design scheme of retaining structure. At present, Coulomb and Rankine earth pressure theories are still widely used because of their simple expressions. However, the semi-infinite space assumption proposed by these two theories makes it not suitable to calculate earth pressure in the cases of narrow backfill. Many studies have shown that the lateral earth pressure of narrow backfill is different from that of semi-infinite-width backfill [1–5].

It should be pointed out that the assumption of the location of the slip surface is fundamental of the earth pressure calculation, and the different calculation results depend on its assumed slip surfaces. In addition to the linear planar slip surface assumed by the classical earth pressure theory, a variety of complex curved slip surface forms have been applied to the calculation model of earth pressure. Some researchers believed that the shape of slip surface should be parabolic [6]. Chen and Snitbhan [7] pointed out that the sliding surface of the backfill behind the retaining wall is circular in the case of ultimate failure. More studies have proved that the logarithmic spiral line or the combination of a logarithmic spiral and straight line is more suitable as an assumed slip surface [8–10]. Further, three-dimensional slip surface is also considered by geotechnical workers [11, 12]. Nevertheless, the above assumed slip surface shape

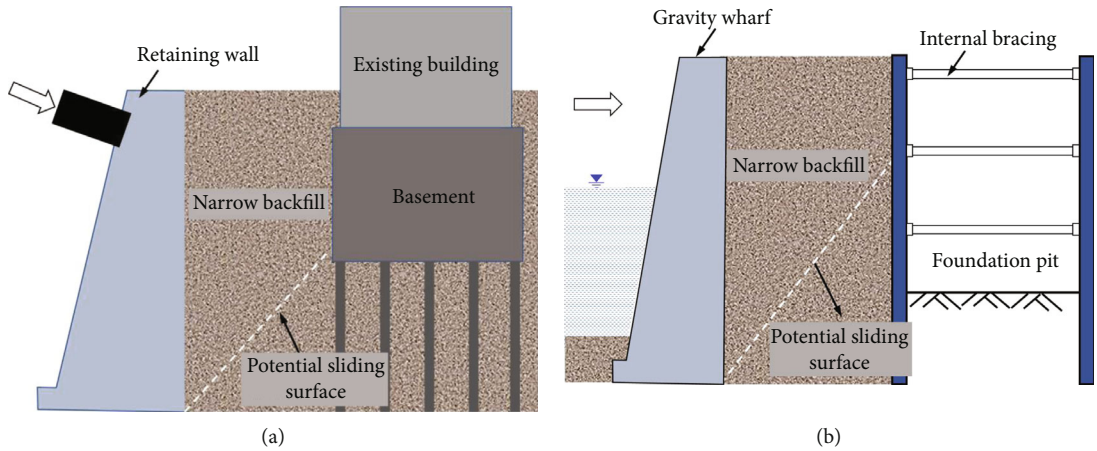

Figure 1: A schematic for narrow width backfill behind a retaining wall: (a) near an existing building; (b) near a foundation pit.

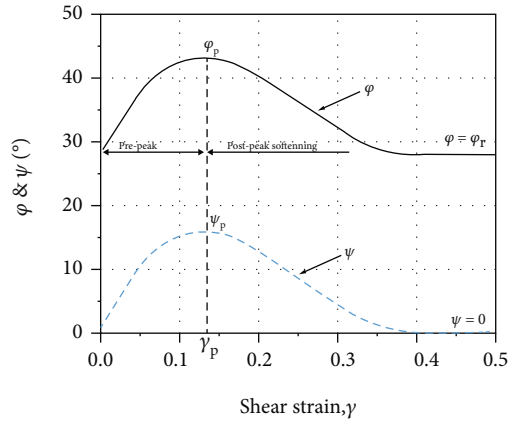

Figure 2: φ and ψ versus shear strain.

requires that the backfill extends to a sufficient distance from the wall to allow for the slip surface to fully develop. When the walls of adjacent existing underground buildings interfere with the full development of the sliding surface, the sliding surface will be cut off or formed into other shapes has always been the focus of earth pressure research. A simple method is to assume that the linear sliding surface is truncated by the adjacent wall to form a trapezoidal sliding wedge [13]. Greco [14] believed that the linear sliding surface will develop to the ground in the form of multisegment broken lines between two adjacent walls. Chen et al. [15, 16] also observed the reflection phenomenon of sliding surfaces in narrow backfill through FELA software. Yang et al. [17] conducted a series of model tests and found that the slip surfaces are curvilinear planes developed from the heel of the retaining wall to the crest of the backfill. Then a variational limit equilibrium method is used to prove that the curvilinear planes agree well with a logarithmic spiral plane.

In these studies on the lateral earth pressure of narrow backfill, scholars pay much more attention to the active earth pressure than the passive earth pressure. In fact, due to the small angle between the sliding surface and the horizontal plane under passive earth pressure, it is more likely to be affected by adjacent underground buildings, as shown in Figure 1. Ying et al. [18] conducted a series of model tests with different widths of backfill for the passive case of a rigid retaining wall, and a slip surface from the wall heel to the intersection with the fixed boundary was observed using particle image velocimetry (PIV) techniques. In recent years, PIV technology is widely used in geotechnical engineering research to obtain soil displacement field [19]. Nevertheless, since the material used in the test is loose sand, when the backfill was compressed by two walls, the strength attenuation of cohesionless backfill has not occurred. However, a large number of triaxial tests show that when the shear strength of dense sand reaches the peak, strain-softening behavior will occur, and the strength of sand will decay [20–24]. In addition, the research on dynamic crushing of sand particles is also under way [25]. The Mohr-Coulomb failure criterion is mostly used in most soil failure problems include passive earth pressure [26], but the postpeak strain-softening behavior of the sandy soil was not considered in the criterion. At present, some constitutive models and analysis methods considering soil strain-softening have been proposed. Wood et al. [27] suggested the idea that the peak stress ratio varies with the state parameter. Li et al. [28] modified a bounding-surface hypoplasticity model and presented a framework for modeling mechanical behavior of sand over a wide range of densities and pressures. Dafalias and Manzari [29] proposed the bounding-surface formulation considering the dependence of plastic potential. Although these models can better reflect the strain-softening behavior of sand, their complex expressions and many parameters make it difficult to be applied to engineering practice.

The main objective of the present study is to propose a simple solution for evaluating the passive earth pressure exerted by narrow backfill considering soil strain-softening. In order to accomplish this, the paper has been organized in the following way. Firstly, a practical model is introduced, which can obtain the internal friction angle at any displacement after peak softening from the stress-strain curve of dense sand triaxial test. Then, the model is verified by the DEM biaxial test of dense sand. Meanwhile, DEM is also used to analyze the variation law of passive earth pressure with the movement of retaining wall and the shape of sliding

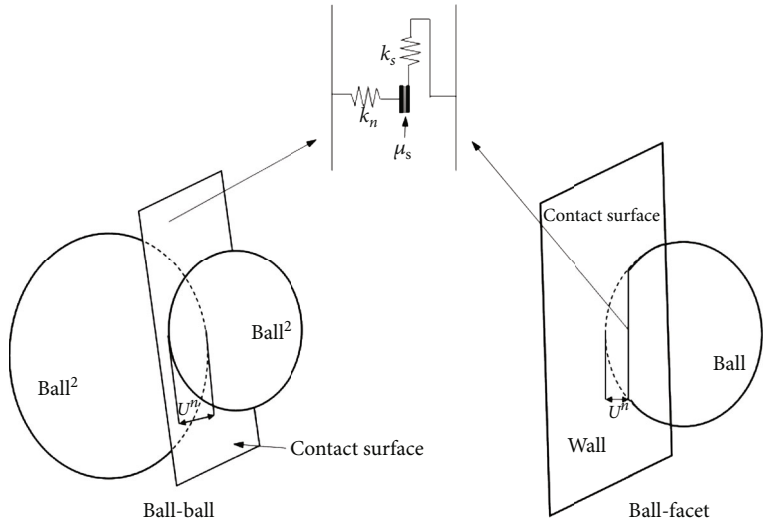

Figure 3: Schematic of substantial contact model in PFC.

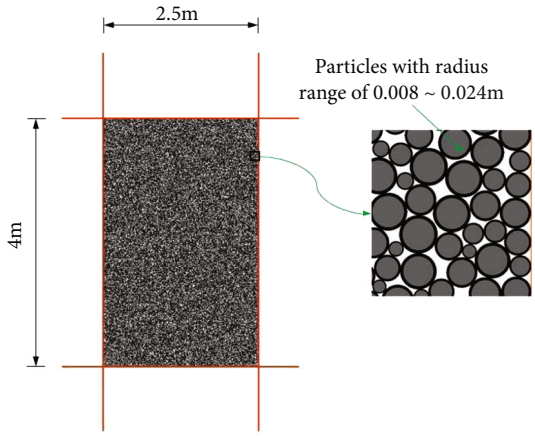

Figure 4: PFC model for biaxial test.

Table 1: Micromaterial parameters of the PFC model.

Parameter	ρ (g/cm^3)	k_n (N/m^2)	k_s (N/m^2)	μ_s	n
Soil	2.65	2×10^7	1.5×10^7	0.75	0.15
Wall	—	2×10^8	1.5×10^8	0.15	—

surface under the condition of narrow backfill. Finally, based on the shape of slip surface obtained by DEM, a simple calculation method of passive earth pressure on retaining walls of narrow backfill width is proposed by using the limit equilibrium method.

2. A Practical Model for Strain-Softening of Dense Sand

The Mohr-Coulomb model used in classical earth pressure theory is a fully elastic-plastic model that assumes constant values of the angle of internal friction and cohesion. The limitation of this assumption is that the weakening of soil strength caused by large displacement is not considered. This calculation method of overestimating the internal friction angle of soil may lead to the safety factor of support structure in practical engineering is far less than that calculated. Roy et al. [30] proposed a modified Mohr-Coulomb model to capture the strain-softening behavior of dense sand, as shown in Figure 2. They believed that with the increase of shear strain, the variation of shear stress can be divided into prepeak stage and postpeak softening stages with the peak value of shear stress as the boundary. In the prepeak stage, the internal friction angle φ and dilatancy angle ψ increase with the increase of shear strain γ, and the shear strength gradually develops. When the shear strain γ exceeds the peak strain γ_p, with the increase of shear strain γ, the internal friction angle φ and dilatancy angle ψ gradually decrease, the internal friction angle φ tends to be stable, and the dilatancy angle ψ will decay to zero.

In order that the proposed model can be more directly applied to the calculation of passive earth pressure, it is necessary to propose a formula that ignores the essence and is directly used for the numerical prediction of internal friction angle. The mathematical function similar to that proposed by Lo and Xu [31] is used to simulate the variation law of internal friction angle after strain-softening of dense sand. The internal friction angle φ corresponding to the postpeak strain can be given as follows:

$$\varphi = \varphi_{\mathrm{p}} - \left(\varphi_{\mathrm{p}} - \varphi_{\mathrm{r}}\right)\left\{1 - \exp\left[-\kappa\left(\varepsilon_{\mathrm{a}} - \varepsilon_{\mathrm{ap}}\right)^2\right]\right\}, \quad (1)$$

where φ is the actual internal friction angle, φ_p is the peak friction angle, and φ_r is the residual internal friction angle, and ε_a and ε_{ap} are the axial strain and axial strain peak of triaxial tests, respectively. The only additional parameter κ can also be approximated by the postpeak portion of the stress-strain curve obtained from laboratory triaxial tests. It should be noted that the error of parameter κ will not have a great impact on the φ value. Therefore, only a few triaxial tests are needed to estimate the value of κ, and then the φ can be calculated by other known parameters.

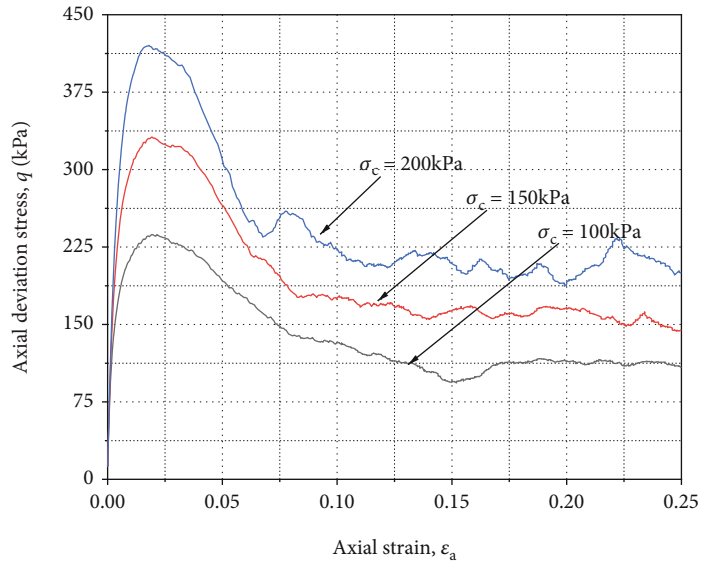

Figure 5: The stress-strain curves of biaxial tests.

3. Numerical Modeling by Using DEM and Verification

3.1. PFC-2D. In recent years, the discrete element method (DEM) has been increasingly favored by geotechnical researchers because of its advantages in simulating granular materials [32–36]. The Particle Flow Code (PFC) is a mesoanalysis software based on the general discrete element model framework, which is mainly used to simulate the motion and interaction of finite size particles. It allows discrete particles to translate and rotate and can automatically identify new contacts. The motion of each particle under the action of unbalanced force and unbalanced moment follows Newton's second law of motion. After the new contact is formed, a new contact force is generated based on the force-displacement law. Furthermore, in PFC, all deformation can only occur in rigid substantial contact, and Figure 3 shows the two contact modes of ball-ball and ball-wall contacts in PFC. Therefore, the deformation and contact stress of particles can be described only by some micromechanical parameters; they can be expressed as the following equations:

$$\begin{aligned} F_n &= k_n U^n, \\ \Delta F_s &= -k_s \Delta U^s, \\ F_s^{\max} &= \mu_s |F_n|, \end{aligned} \tag{2}$$

where k_n, k_s, and μ_s are the microparameter set in PFC, representing the normal stiffness, the tangential stiffness, and the friction coefficient; F_n and U^n are the normal stress and the normal displacement; ΔF_s and ΔU^s are the increments of the tangential stress and the tangential relative displacement; $F_s^{\max}$ is the maximum allowable tangential stress on contact surface.

Compared with the numerical simulation method based on continuous medium theory, PFC is not limited by deformation and can easily deal with noncontinuum media mechanic problems, such as the large deformation problems of sand [37–39]. Additionally, the particle flow program integrates two-dimensional (PFC-2D) and three-dimensional (PFC-3D). Compared with PFC-3D model, although there are fewer particles in PFC-2D model, it has certain advantages in analyzing the earth pressure problem [40, 41] assumed to be plane strain.

3.2. Biaxial Test by Using PFC-2D. Figure 4 shows the biaxial test model established by PFC-2D; the micromaterial parameters used in the model are shown in Table 1. A sufficient number of particles (number of particles = 9,726) were generated in the biaxial sample with a height of 4 m and a width of 2.5 m. It is worth pointing out that due to the difference in the seepage threshold of the 2D model and the 3D model, the porosity of the 2D model is much smaller than that of the 3D model, and the value is generally between 0.15 and 0.2 [42, 43]. Considering the stress state of the backfill soil behind the wall in the subsequent earth pressure model, the confining pressures of the three biaxial tests were 100 kPa, 150 kPa, and 200 kPa, respectively.

The stress-strain curves of biaxial tests are shown in Figure 5. It is obvious that the strain-softening behavior becomes more obvious with the increase of confining pressure, and the same results were obtained in previous tests [30, 31]. By comprehensively analyzing the stress-strain curves of different biaxial tests, a value of 300 was selected for κ. Although different stress states will have different κ values, the author suggests that the same soil sample can choose a representative κ value within a certain stress range for ease of use. In addition, the fitting effect of κ taking 300 on the three curves is not the best, but it is sufficiently representative as a representative value. Using the peak internal

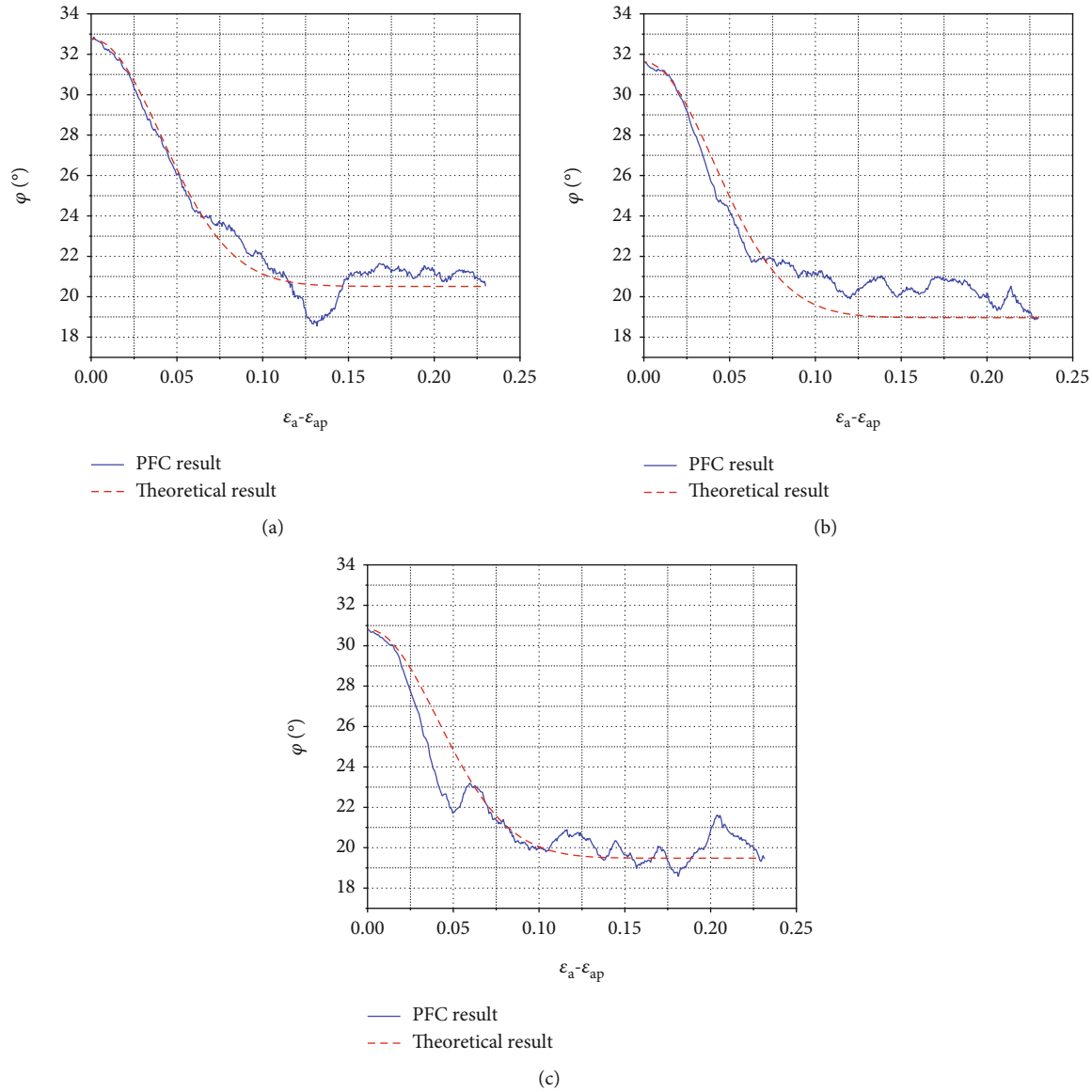

Figure 6: φ versus $\varepsilon_a - \varepsilon_{ap}$ after peak value: (a) $\sigma_c = 100$ kPa; (a) $\sigma_c = 150$ kPa; (a) $\sigma_c = 200$ kPa.

friction angle φ_p and residual internal friction φ_r angle calculated by the biaxial test, the variation law of internal friction angle φ with axial strain in the post peak stage is drawn based on Equation (1), as shown in Figure 6. The internal friction φ corresponding to each axial strain ε_a in the biaxial test can be derived as follows:

$$\varphi = \arcsin \frac{q}{p'} = \arcsin \frac{\sigma_1 - \sigma_3}{\sigma_1 + \sigma_3}. \quad (3)$$

It can be seen from Figure 6 that although the PFC results have great fluctuation due to their own working characteristics, the test results are still in good agreement with the calculation results of the formula. Additionally, it can be seen that the peak internal friction angle decreases slightly with the increase of confining pressure. And Bolton [44, 45] believed that high confining pressure will reduce the dilatancy angle of sand.

3.3. DEM Analysis of Passive Earth Pressure on Retaining Wall of Narrow Backfill. The retaining wall model is 7 m high and 3 m wide (number of particles = 17,463), and the backfill depth along the moving retaining wall is 5 m, as shown in Figure 7. Unlike the motion of particles, which must follow Newton's law of motion, the motion of the wall is specified by the user. Making the rigid wall slowly move towards the backfill through the instruction and using the information recording tool "history" in the program to obtain the change of the total horizontal contact force of the rigid wall with the displacement during the translation process are shown in Figure 8. With the movement of the retaining wall, the earth pressure behind the wall gradually increased. When a certain displacement is reached (about

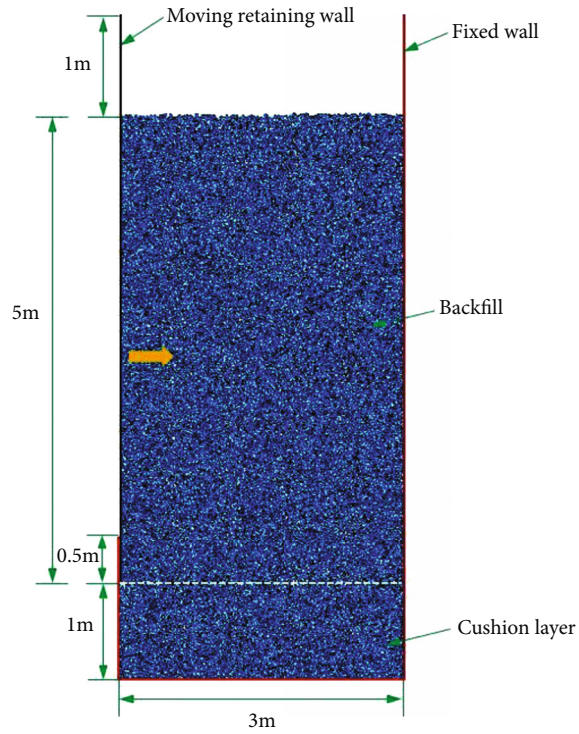

Figure 7: PFC model for soil behind retaining wall.

0.03 H in the test), the earth pressure reached its peak value, that is, it reached the passive limit state. In the passive earth pressure research that has been carried out, it is generally believed that after reaching the passive limit state, the earth pressure will remain unchanged with the movement of the retaining wall [18, 46–48], and the passive earth pressure value is also taken for calculation in relevant design. However, it can be seen in Figure 8 that after reaching the passive earth pressure, the value of lateral earth pressure tends to decrease as the retaining wall continues to move. The attenuation mode is similar to the variation law of axial stress with axial strain in the biaxial test of strain-softening soil analyzed earlier. The reason is that in the narrow backfill, with the large movement of the retaining wall to the soil, the backfill behind the wall will be squeezed, and the extrusion stress of the soil behind the wall, especially the soil with large buried depth, will also produce strain-softening behavior. Then the internal friction angle decreases, resulting in the lateral earth pressure being less than the passive earth pressure in the limit state. In the model, the backfill width is very small. When the displacement of the retaining wall is too large, the backfill surface will rise, so the rise of the resultant force of lateral earth pressure can be observed in Figure 8.

The displacement field of soil can be analyzed by the color of particles using "ball displacement mag." As show in Figure 9, the displacement of the particles in the dark blue zone is almost close to zero, and this area can be identified as a stationary region. The area of other color particles can be identified as the moving region. The slip surface of the soil is interpreted as the boundary between the stationary region and moving region. The similar way has been used by previous literatures [41, 49]. In addition, it should be pointed out that when the soil reaches the passive limit state, as the retaining wall continues to move, although the displacement of particles in the moving area increases, the size of the moving area does not change, and the position of the sliding surface does not change. It is well known that in the traditional theory of earth pressure, the sliding surface of the backfill changes with the change of the internal friction angle. Therefore, when calculating the passive earth pressure after soil strain softening, it is necessary to use the peak internal friction angle to calculate the position of the sliding surface first and then use the actual internal friction angle to calculate the earth pressure.

4. Analytical Solution to Passive Earth Pressure

As shown above, after the narrow backfill retaining wall reaches the passive limit state, the sliding surface is a plane intersecting with the wall of the existing building through the wall heel. The sliding wedge is a trapezoidal body with sliding surface, retaining wall and fixed wall as the boundary, and this is consistent with the experimental observation of Ying et al. [18]. The calculation model is schematically shown in Figure 10, and the sliding wedge ABCD moves upward along the three boundaries. The external forces acting on the sliding wedge include W, E_p, E_1, and R. Herein, W is the self-weight of the sliding wedge, E_p is the reaction force of retaining wall, E_1 is the reaction force of fixed wall, and R is the reaction force of sliding wedge. In the figure, θ is the angle between the sliding surface and the horizontal plane, the included angle between R and the normal of the sliding surface is the internal friction angle φ, and the included angles δ and δ_1 between E_p and E_1 and the horizontal plane are the interface friction angles of moving retaining wall and fixed wall, respectively.

The equilibrium equations of ABCD in x and z direction can be expressed as

$$E_p \cos\delta - R\sin(\theta+\varphi) = E_1\cos\delta_1, \tag{4}$$

$$W + E_p \sin\delta + E_1\sin\delta_1 = R\cos(\theta+\varphi). \tag{5}$$

The self-weight of the soil wedge can be obtained from the geometric relationship:

$$W = \gamma BH - \frac{1}{2}\gamma B^2 \tan\theta, \tag{6}$$

where γ is the unit weight of the backfill, B is the distance between retaining wall and fixed wall, H is the height of the retaining wall.

Although the reaction force of the fixed wall is assumed to be static earth pressure in some literatures, it is found that the reaction force increases gradually with the movement of the retaining wall in the PFC simulation process. Therefore,

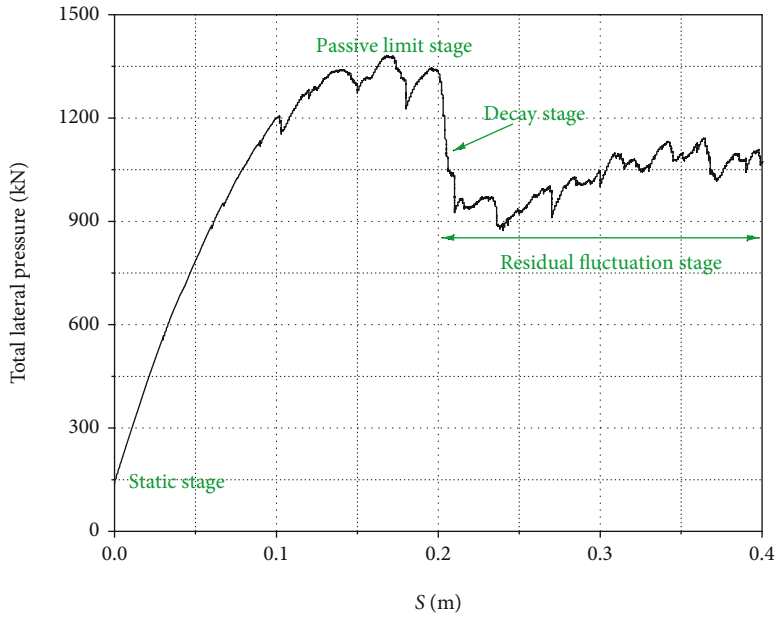

Figure 8: Total lateral pressure versus displacement of the wall.

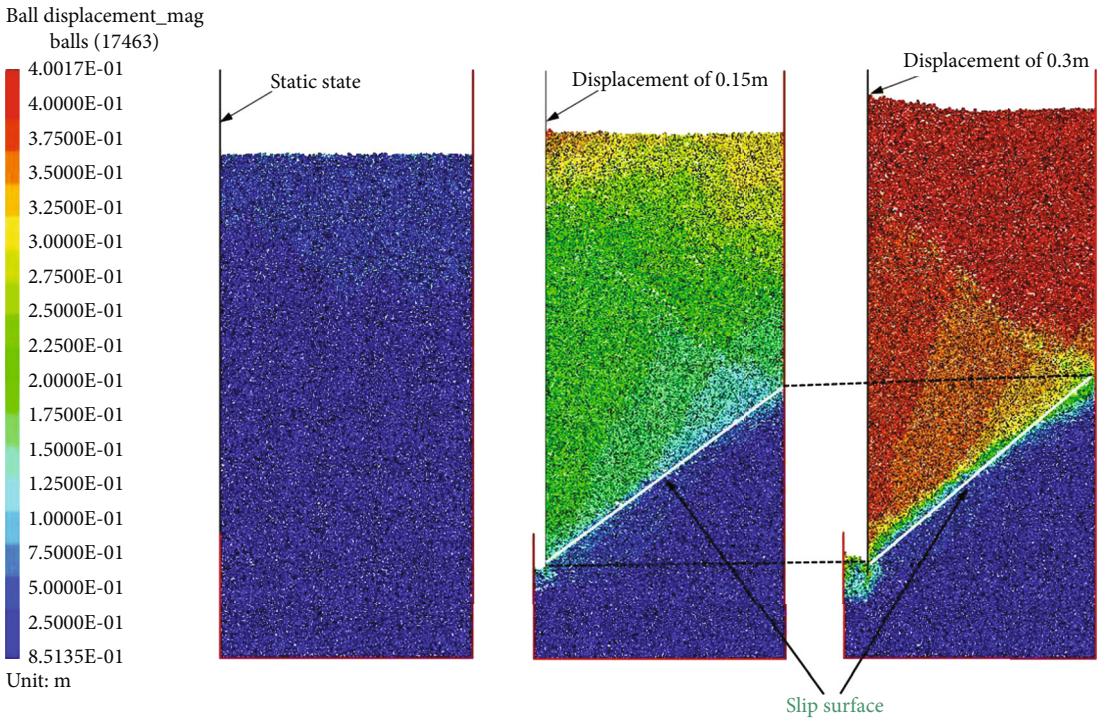

Figure 9: Variation of soil displacement field behind retaining wall.

the Coulomb passive earth pressure is more suitable for calculating the reaction force in the area than static earth pressure. E_1 can be obtained from the following equation:

$$E_1 = \frac{1}{2}K_p\gamma(H - B\tan\theta)^2, \tag{7}$$

where K_p is the Coulomb passive earth pressure coefficient.

By substituting Equations (6) and (7) into Equations (3) and (5), the resultant of active earth pressure acting on the rigid retaining wall can be obtained as follows:

$$E_p = \frac{\left(\gamma BH - (1/2)\gamma B^2\tan\theta\right)\sin(\theta+\varphi)}{\cos(\delta+\theta+\varphi)} + \frac{K_p\gamma(H - B\tan\theta)^2\cos(\delta_1-\theta-\varphi)}{2\cos(\delta+\theta+\varphi)}. \tag{8}$$

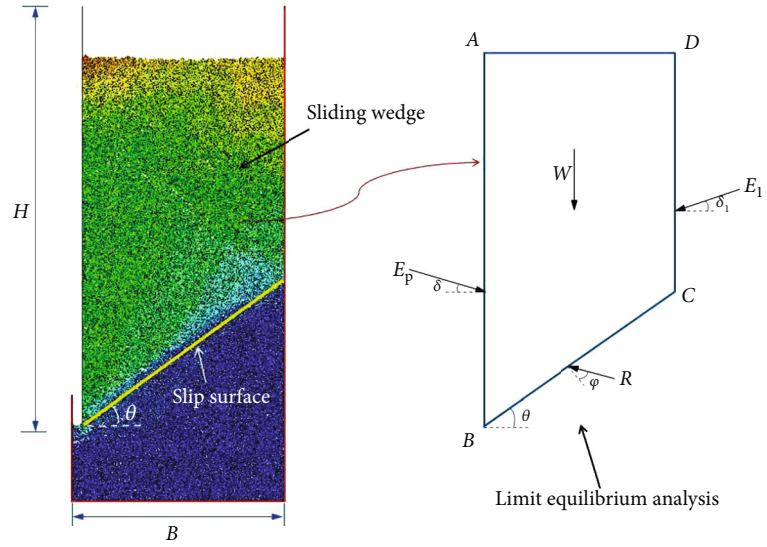

Figure 10: Schematics of calculation model.

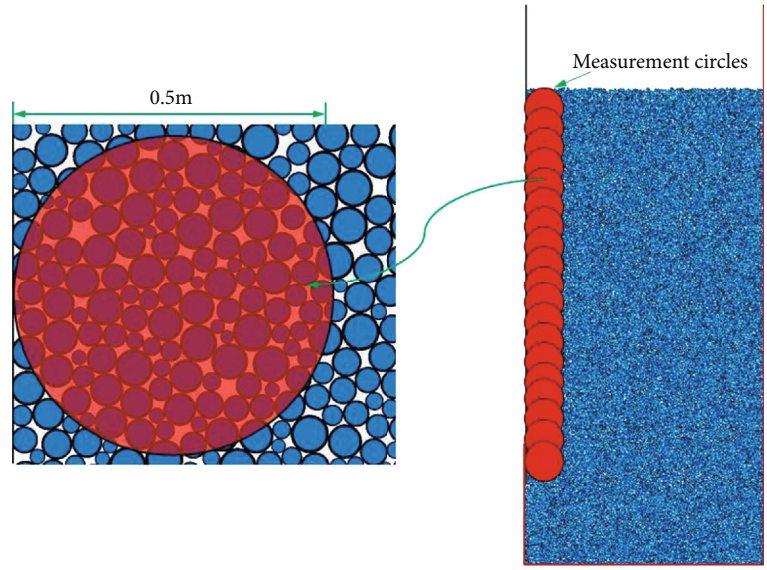

Figure 11: Layout of measuring circles.

The above θ value can be obtained by minimizing E_p. It should be noted that when solving θ, the internal friction angle value in Equation (9) should take the peak internal friction angle φ_p. The "programming solution" tool of Microsoft Excel is used to conveniently minimize E_p.

The passive earth pressure distributions along the depth can be expressed as

$$p_p = \frac{(2\gamma BH - \gamma B^2 \tan\theta)\sin(\theta+\varphi)}{\cos(\delta+\theta+\varphi)H^2} z + \frac{K_p \gamma (H - B\tan\theta)^2 \cos(\delta_1 - \theta - \varphi)}{\cos(\delta+\theta+\varphi)H^2} z. \quad (9)$$

Furthermore, in order to calculate the passive earth pressure of narrow backfill after strain-softening more easily, based on Equation (9), the displacement of the retaining wall is in the horizontal direction, corresponding to the backfill width B. The axial strain ε_a in the triaxial test can be replaced by S/B. The actual internal friction angle after the passive limit state is expressed by a mathematical function similar to Equation (9):

$$\varphi = \varphi_p - (\varphi_p - \varphi_r)\left(1 - e^{-\kappa\left((S-S_p)/B\right)^2}\right). \quad (10)$$

where S_p is the displacement of retaining wall in passive limit state.

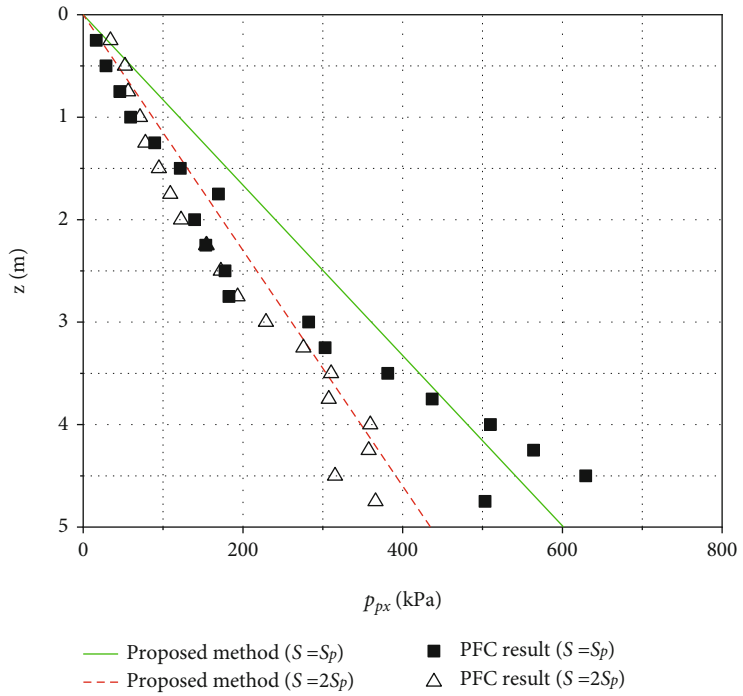

Figure 12: Comparison of the distribution of passive earth pressures along depth between the theoretical solution and PFC results.

5. Result Analysis

To verify the necessity of the proposed theory, a comparison analysis with the numerical simulation results was conducted. Nineteen measurement circles with a radius of 0.25 m were arranged tangent to retaining wall from top to bottom as shown in Figure 11 to measure the mean lateral stress in the zones. Using the fish language in PFC to write the program, the measuring circles will be deleted after the measured stress. When it is generated again, the position will change and continue to be tangent to the retaining wall. The mean lateral stress measured by each measurement circle is the lateral earth pressure corresponding to the height of the center of the circle. In order to ensure that the number of measurement points and the number of particles in the measurement circles are met, the measurement area of adjacent measurement circles overlaps by half. The radius of the measurement circles is more than ten times of the maximum particle radius; it is considered that the measurement results are accurate enough. Figure 12 shows the comparison of the distribution of passive earth pressures along depth between the theoretical solution and numerical simulation results. When the displacement of the retaining wall exceeds the passive limit displacement, if the weakening of the strength caused by strain-softening is not considered, and the passive earth pressure in the limit state is continued to be used for engineering design, the value of the earth pressure behind the wall will be overestimated, resulting in hidden dangers of engineering safety.

In addition, the effect of fill width and strain-softening behavior on passive earth pressure is the gravity of this paper. In order to analyze the influence effect of the two factors, parameter analysis is carried out, in which the basic

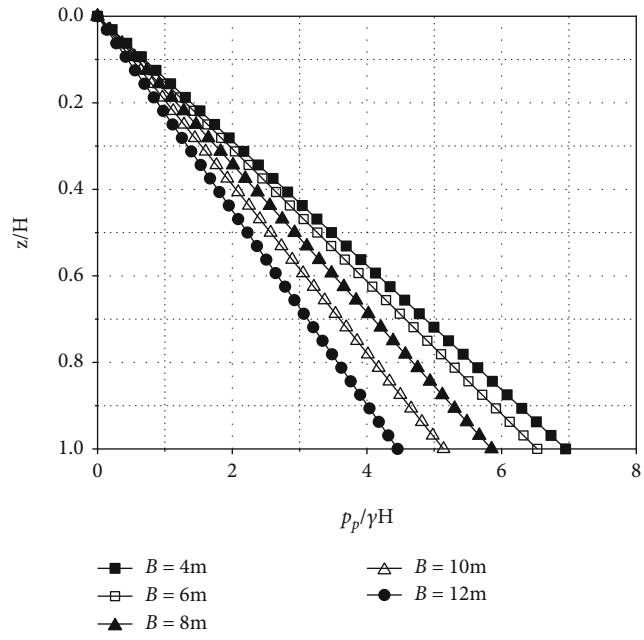

Figure 13: $p_p/\gamma H$ versus z/H for the different backfill widths B.

parameters are given as follows: $H = 8$ m, $\gamma = 18.5$ kN/m^3, $\varphi_p = 33^\circ$, $\varphi_r = 20^\circ$, $\delta = \varphi_p/3$, $S_p = 0.03H$, and $\kappa = 300$.

Figure 13 shows the normalized passive earth pressure distribution ($p_p/\gamma H$) along the normalized depth (z/H) for different values of the widths of backfill, various values of B varying from 4 m to 12 m. As seen in Figure 13, it is obvious that passive earth pressure significantly decreases as B increases. Furthermore, when the backfill width exceeds the height of the retaining wall ($B = 10$ and $B = 12$ m), the

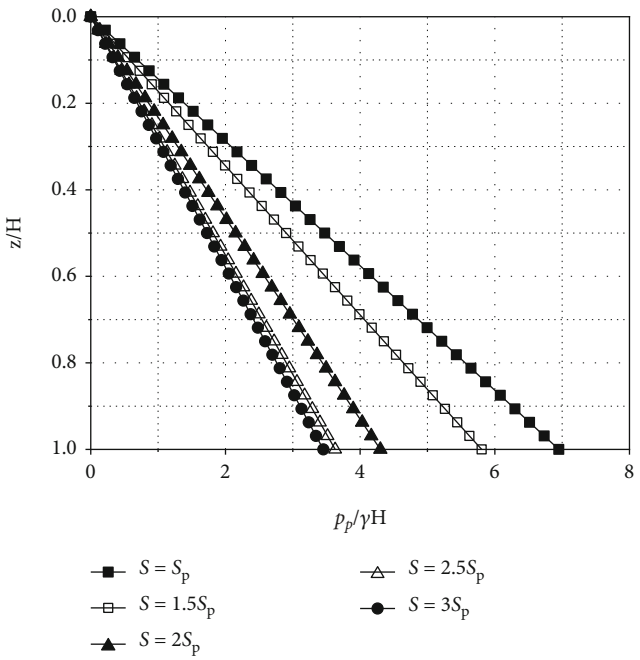

Figure 14: $p_p/\gamma H$ versus z/H for the different displacements S after passive limit state.

passive earth pressure will continue to decrease with the increase of the backfill width, indicating that the backfill width is still narrow backfill for the passive earth pressure. Passive earth pressure is more sensitive to adjacent underground buildings, and the influence of underground buildings with a certain distance on the value of passive earth pressure still needs to be considered.

In order to study the effect of the displacement after passive limit state on the passive earth pressure against the retaining wall, different values of S (i.e., $S = S_p$, $1.5S_p$, $2S_p$, $2.5S_p$, $3S_p$) were used. The change of passive earth pressure along the depth is shown in Figure 14. Figure 14 indicates that passive earth pressure marginally decreases with the increasing value of S, and the attenuation is less obvious when the S value is larger. It can be explained that when the S value is large, the internal friction angle of the fill is close to the residual internal friction angle, and the attenuation of the internal friction angle becomes slower.

6. Conclusions

The estimation of passive earth pressure has always been a focus in the field of geotechnical engineering, and different analysis methods are needed in different situations. Based on the limit equilibrium method, a new simple analysis method of passive earth pressure of narrow backfill considering strain-softening is proposed in this paper. The new method uses DEM to verify the proposed strain-softening model and determine the location of the slip surface. Furthermore, the effect of the backfill width and the displacement after passive limit state on the distribution of passive earth pressures along the depth was also discussed. The main conclusions of this study are summarized below:

(1) In the same way that the internal friction angle decreases due to strain softening after the axial strain reaches the limit in the triaxial test, the passive earth pressure of narrow backfill will also decay with the displacement of the retaining wall after the passive limit state

(2) The passive sliding surface of narrow backfill is a plane intersecting with the wall of the existing building through the wall heel. Additionally, excessive displacement will reduce the passive earth pressure but will not change the position of the sliding surface

(3) The passive earth pressure decreases as the widths of backfill and the displacement after passive limit state increases. Compared with active earth pressure, passive earth pressure is more easily affected by adjacent underground buildings

Data Availability

The data used to support the findings of this study are included within the article.

Conflicts of Interest

The authors declare that they have no conflicts of interest to report regarding the present study.

Acknowledgments

This research was supported by the National Natural Science Foundation of China (NSFC) (Grant No. 51678230) and the Science Foundation for Youths of Hunan Province of China (Grant No. 2021JJ40460), which are gratefully acknowledged.

References

[1] R. L. Handy, "The arch in soil arching," *Journal of Geotechnical Engineering*, vol. 111, no. 3, pp. 302–318, 1985.

[2] S. Frydman and I. Keissar, "Earth pressure on retaining walls near rock faces," *Journal of Geotechnical Engineering*, vol. 113, no. 6, pp. 586–599, 1987.

[3] W. A. Take and A. J. Valsangkar, "Earth pressures on unyielding retaining walls of narrow backfill width," *Canadian Geotechnical Journal*, vol. 38, no. 6, pp. 1220–1230, 2001.

[4] C. C. Fan and Y. S. Fang, "Numerical solution of active earth pressures on rigid retaining walls built near rock faces," *Computers and Geotechnics*, vol. 37, no. 7-8, pp. 1023–1029, 2010.

[5] H. Liu and D. Z. Kong, "Active earth pressure of finite width soil considering intermediate principal stress and soil arching effects," *International Journal of Geomechanics*, vol. 22, no. 3, article 04021294, 2022.

[6] S. Goel and N. R. Patra, "Effect of arching on active earth pressure for rigid retaining walls considering translation mode," *International Journal of Geomechanics*, vol. 8, no. 2, pp. 123–133, 2008.

[7] W. F. Chen and N. Snitbhan, "On slip surface and slope stability analysis," *Soils and Foundations*, vol. 15, no. 3, pp. 41–49, 1975.

[8] J. Kumar, "Seismic passive earth pressure coefficients for sands," *Canadian Geotechnical Journal*, vol. 38, no. 4, pp. 876–881, 2001.

[9] A. H. Soubra and B. Macuh, "Active and passive earth pressure coefficients by a kinematical approach," *Proceedings of the Institution of Civil Engineers. Geotechnical Engineering*, vol. 155, no. 2, pp. 119–131, 2002.

[10] Y. Xie and B. Leshchinsky, "Active earth pressures from a log-spiral slip surface with arching effects," *Géotechnique Letters*, vol. 6, no. 2, pp. 149–155, 2016.

[11] A. H. Soubra and P. Regenass, "Three-dimensional passive earth pressures by kinematical approach," *Journal of Geotechnical and Geoenvironmental Engineering*, vol. 126, no. 11, pp. 969–978, 2000.

[12] S. Benmebarek, T. Khelifa, N. Benmebarek, and R. Kastner, "Numerical evaluation of 3D passive earth pressure coefficients for retaining wall subjected to translation," *Computers and Geotechnics*, vol. 35, no. 1, pp. 47–60, 2008.

[13] J. J. Chen, M. G. Li, and J. H. Wang, "Active earth pressure against rigid retaining walls subjected to confined cohesionless soil," *International Journal of Geomechanics*, vol. 17, no. 6, p. 06016041, 2017.

[14] V. Greco, "Active thrust on retaining walls of narrow backfill width," *Computers and Geotechnics*, vol. 50, pp. 66–78, 2013.

[15] F. Q. Chen, Y. J. Lin, and D. Y. Li, "Solution to active earth pressure of narrow cohesionless backfill against rigid retaining walls under translation mode," *Soils and Foundations*, vol. 59, no. 1, pp. 151–161, 2019.

[16] F. Q. Chen, J. T. Yang, and Y. J. Lin, "Active earth pressure of narrow granular backfill against rigid retaining wall near rock face under translation mode," *International Journal of Geomechanics*, vol. 19, no. 12, article 04019133, 2019.

[17] M. H. Yang, X. C. Tang, and Z. Y. Wu, "Slip surface and active earth pressure of cohesionless narrow backfill behind rigid retaining walls under translation movement mode," *International Journal of Geomechanics*, vol. 20, no. 8, article 04020115, 2020.

[18] H. W. Ying, J. H. Zhang, X. G. Wang, B. H. Li, and W. Zhu, "Experimental analysis of passive earth pressure against rigid retaining wall under translation mode for finite soils," *Chinese Journal of Geotechnical Engineering*, vol. 38, no. 6, pp. 978–986, 2016.

[19] B. X. Yuan, Z. J. Li, W. J. Chen et al., "Influence of groundwater depth on pile–soil mechanical properties and fractal characteristics under cyclic loading," *Fractal and Fractional*, vol. 6, no. 4, p. 198, 2022.

[20] F. Tatsuoka and K. Ishihara, "Yielding of sand in triaxial compression," *Soils and Foundations*, vol. 14, no. 2, pp. 63–76, 1974.

[21] M. G. Jefferies, "Nor-sand: a simle critical state model for sand," *Géotechnique*, vol. 43, no. 1, pp. 91–103, 1993.

[22] X. S. Li and Y. F. Dafalias, "Dilatancy for cohesionless soils," *Géotechnique*, vol. 50, no. 4, pp. 449–460, 2000.

[23] T. Omar and A. Sadrekarimi, "Specimen size effects on behavior of loose sand in triaxial compression tests," *Canadian Geotechnical Journal*, vol. 52, no. 6, pp. 732–746, 2015.

[24] A. Strahler, A. W. Stuedlein, and P. W. Arduino, "Stress-strain response and dilatancy of sandy gravel in triaxial compression and plane strain," *Journal of Geotechnical and Geoenvironmental Engineering*, vol. 142, no. 4, article 04015098, 2016.

[25] B. X. Yuan, Z. H. Li, Y. M. Chen et al., "Mechanical and microstructural properties of recycling granite residual soil reinforced with glass fiber and liquid-modified polyvinyl alcohol polymer," *Chemosphere (Oxford)*, vol. 286, article 131652, 2022.

[26] H. Long, K. Zhuang, B. Deng, J. L. Jiao, J. J. Zuo, and E. L. You, "Dynamic characteristics of coral sand in the condition of particle breakage," *Geofluids*, vol. 2022, Article ID 5304179, 8 pages, 2022.

[27] D. M. Wood, K. Belkheir, and D. F. Liu, "Strain softening and state parameter for sand modelling," *Géotechnique*, vol. 44, no. 2, pp. 335–339, 1994.

[28] X. Li, Y. Dafalias, and Z. Wang, "State-dependant dilatancy in critical-state constitutive modelling of sand," *Canadian Geotechnical Journal*, vol. 36, no. 4, pp. 599–611, 1999.

[29] Y. F. Dafalias and M. T. Manzari, "Simple plasticity sand model accounting for fabric change effects," *Journal of Engineering Mechanics*, vol. 130, no. 6, pp. 622–634, 2004.

[30] K. Roy, B. Hawlader, S. Kenny, and I. Moore, "Finite element modeling of lateral pipeline–soil interactions in dense sand," *Canadian Geotechnical Journal*, vol. 53, no. 3, pp. 490–504, 2016.

[31] M. J. Iftekhar Alam, S. R. Lo, and C. T. Gnanendran, "Numerical modeling of strain-softening response in triaxial testing of silty sand using FLAC2D," *Soil Behavior and Geomechanics*, vol. 2014, pp. 606–614, 2014.

[32] J. R. Williams and N. Rege, "The development of circulation cell structures in granular materials undergoing compression," *Powder Technology*, vol. 90, no. 3, pp. 187–194, 1997.

[33] B. Le Hello and P. Villard, "Embankments reinforced by piles and geosynthetics–numerical and experimental studies dealing with the transfer of load on the soil embankment," *Engineering Geology*, vol. 106, no. 1-2, pp. 78–91, 2009.

[34] J. H. Yang, S. R. Wang, H. Q. Zhang, and C. Cao, "Particle-scale analysis of key technologies on cut-and-over tunnel in slope engineering," *Journal of Engineering Science and Technology Review*, vol. 7, no. 4, pp. 46–52, 2014.

[35] G. R. McDowell and H. Li, "Discrete element modelling of scaled railway ballast under triaxial conditions," *Granular Matter*, vol. 18, no. 3, pp. 1–10, 2016.

[36] S. F. Sizkow and E. S. Usama, "Discrete-element method simulations of the seismic response of flexible retaining walls," *Journal of Geotechnical and Geoenvironmental Engineering*, vol. 147, no. 2, article 04020157, 2021.

[37] Y. D. Chen, A. Deng, A. T. Wang, and H. S. Sun, "Performance of screw-shaft pile in sand: model test and DEM simulation," *Computers and Geotechnics*, vol. 104, pp. 118–130, 2018.

[38] M. Khanal, M. Elmouttie, B. Poulsen, A. Olsson, and D. Adhikary, "Effect of loading rate on sand pile failure: 2D DEM simulation," *Geotechnical and Geological Engineering*, vol. 35, no. 2, pp. 889–896, 2017.

[39] G. Macaro, S. Utili, and C. M. Martin, "DEM simulations of transverse pipe–soil interaction on sand," *Géotechnique*, vol. 71, no. 3, pp. 189–204, 2021.

[40] M. G. Li, J. J. Chen, and J. H. Wang, "Arching effect on lateral pressure of confined granular material: numerical and theoretical analysis," *Granular Matter*, vol. 19, no. 2, pp. 1–11, 2017.

[41] M. H. Yang and B. Deng, "Simplified method for calculating the active earth pressure on retaining walls of narrow backfill width based on DEM analysis," *Advances in Civil Engineering*, vol. 2019, 12 pages, 2019.

[42] C. Thornton, "Numerical simulations of deviatoric shear deformation of granular media," *Géotechnique*, vol. 50, no. 1, pp. 43–53, 2000.

[43] K. Bagi, "Statistical analysis of contact force components in random granular assemblies," *Granular Matter*, vol. 5, no. 1, pp. 45–54, 2003.

[44] M. D. Bolton, "The strength and dilatancy of sands," *Géotechnique*, vol. 36, no. 1, pp. 65–78, 1986.

[45] S. T. Hsu and H. J. Liao, "Uplift behaviour of cylindrical anchors in sand," *Canadian Geotechnical Journal*, vol. 35, no. 1, pp. 70–80, 1998.

[46] R. G. James and P. L. Bransby, "Experimental and theoretical investigations of a passive earth pressure problem," *Géotechnique*, vol. 20, no. 1, pp. 17–37, 1970.

[47] Y. S. Fang, Y. Y. C. Ho, and T. J. Chen, "Passive earth pressure with critical state concept," *Journal of Geotechnical and Geoenvironmental Engineering*, vol. 128, no. 8, pp. 651–659, 2002.

[48] B. Deng and M. H. Yang, "Analysis of passive earth pressure for unsaturated retaining structures," *International Journal of Geomechanics*, vol. 19, no. 12, article 06019016, 2019.

[49] S. S. Nadukuru and R. L. Michalowski, "Arching in distribution of active load on retaining walls," *Journal of Geotechnical and Geoenvironmental Engineering*, vol. 138, no. 5, pp. 575–584, 2012.